New Results from ZEUS

B. Löhr, on behalf of the ZEUS Collaboration
DESY, Notkestraße 85, 22607 Hamburg, Germany

Recent results from the ZEUS experiment are reviewed. This report concentrates on structure functions at very low Q^2, cross sections at very high Q^2, searches beyond the standard model, jets in DIS and photoproduction, and cross sections and event shapes of diffractive processes.

1. INTRODUCTION

From 1994 to the end of 1997, HERA collided positrons with protons. The ZEUS detector recorded data corresponding to 48.1 pb^{-1} of which 38.4 pb^{-1} come from the 1996 to 1997 running period. This large dataset allowed the exploration of the very high Q^2 kinematic regime. Access to the very low Q^2 and very low x region was made possible by improvements in the instrumentation of the ZEUS detector. Before the start of the 1997 running period, a small silicon tracker hodoscope, the beam pipe tracker (BPT), was installed in front of the existing beam-pipe calorimeter (BPC) which measures scattered positrons at very small angles. The silicon tracker determines precisely the impact point of the scattered positron on the BPC and thus extends the useful area of the BPC towards the geometric bounderies, in particular in the direction closer to the beam. For events without a track detected in the ZEUS central drift chamber, the scattered electron detected in the BPT provides a track to determine the event vertex. This gave access to Q^2 values as low as $Q^2 = 0.045\ \mathrm{GeV}^2$.

2. INCLUSIVE CROSS SECTIONS AND ELECTROWEAK PROCESSES

F_2 at very low Q^2 : The structure function $F_2(x, Q^2)$ has been determined in the range $0.045 < Q^2 < 0.65\ \mathrm{GeV}^2$ from the data taken with the BPC/BPT in 1997. Figure 1 shows $F_2(x, Q^2)$ as a function of x in different Q^2 intervals. The data are compared to predictions from several parametrizations of $F_2(x, Q^2)$. The REGGE based parametrizations and fits [1][2][4] can describe the data up to about $Q^2 = 0.5\ \mathrm{GeV}^2$. The ALLM97 [3] parametrization gives an adequate despription for $Q^2 \geq 0.2\ \mathrm{GeV}^2$.
Figure 2 shows the virtual photon-proton cross sections extracted from these data together with ZEUS [5] and H1 [6] data at higher Q^2. The curves shown correspond to the same parametrizations and fits as in figure 1. The ZEUS and H1 measurements of the photoproduction cross section are also shown. The extrapolations of the very low Q^2 data to $Q^2 = 0$ lie somewhat above the directly measured photoproduction cross sections.

F_2 in the full kinematic region : The determination of $F_2(x, Q^2)$ over the full kinematical region is still preliminary. From Fig.3 it can be seen that a wide range in x and Q^2 is now covered by the results from ZEUS. These data match well with BCDMS [7], E665 [8], and NMC [9] data measured in fixed target experiments.

Contribution of charm to $F_2(x, Q^2)$: A prominent feature of $F_2(x, Q^2)$ in the kinematical range of HERA is the strong rise of $F_2(x, Q^2)$ when x decreases at fixed Q^2. This rise is connected to the rise of the gluon density in the proton. The production of charm quarks proceeds predominantly via photon-gluon fusion and thus also depends on the gluon density. The cross section for $D^{*\pm}$ electroproduction in the region $1 < Q^2 < 600\ \mathrm{GeV}^2$; $0.02 < y < 0.7$ and $|\eta(D^{*\pm})| < 1.5$; $1.5 < p_T(D^{*\pm}) < 15$ GeV has been determined:

$$\sigma(e^+p \to e^+D^{*\pm}X) = 8.31 \pm 0.31(\mathrm{stat.})\ ^{+0.30}_{-0.50}(\mathrm{sys.})\ \mathrm{nb.}$$

Differential cross sections agree well with NLO calculations as implemented in the HVQDIS program [10] for the charm quark mass range $1.3\ \mathrm{GeV} < m_c < 1.5\ \mathrm{GeV}$ and after inclusion of "beam-drag" effect in which color strings drag the

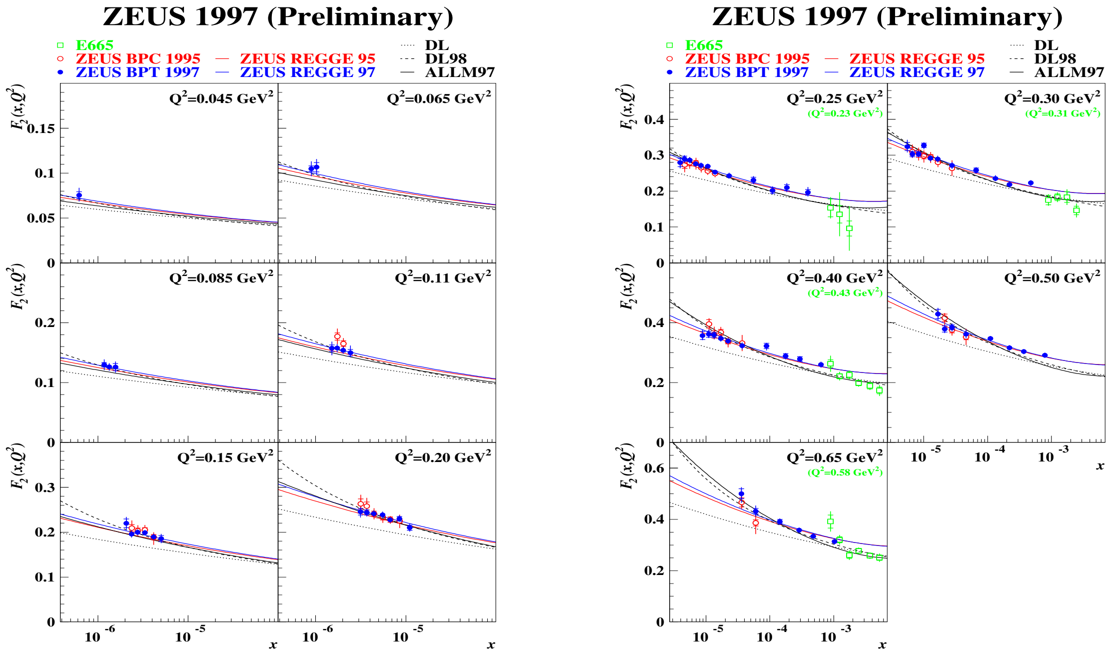

Figure 1. $F_2(x, Q^2)$ from ZEUS for the 1995 dataset and the 1998 dataset in the kinematic region of the BPC. In addition, data from E665 at higher x are shown in some Q^2 intervals. The data are compared with predictions of several parametrizations of $F_2(x, Q^2)$: DL [1], DL98 [2], ALLM97 [3], and ZEUS fits ZEUS REGGE95 [4] and preliminary ZEUS REGGE97.

charmed system towards the proton remnant direction. The model was used to extrapolate the measured values to the whole kinematic range in p_T and $\eta(D^{*\pm})$. In Fig.4, the charm fraction of the total $F_2(x, Q^2)$ structure function is given for several values of Q^2 as a function of x. For fixed Q^2, it increases with decreasing x, which means that the charm contribution rises faster than the total $F_2(x, Q^2)$, in agreement with pQCD. The fraction of charm also increases with Q^2 reaching values as high as 30% at Q^2 of 130 GeV^2.

Neutral and charged current cross sections at high Q^2 : The analyses of the neutral current and charged current cross sections in e^+p-scattering up to the highest Q^2 have been finalized. No deviations from the Standard Model were observed in the single differential cross sections. The data taken in 1998 and 1999 on e^-p-scattering allow a comparison of e^-p with e^+p cross sections. Figure 5 shows the ratio $d\sigma/dQ^2(e^-)/d\sigma/dQ^2(e^+)$ for charged current events. The ratio is greater than 1 at Q^2 =1 GeV^2 and rises at higher Q^2. This can be understood from the dependence of the cross sections on the parton distributions in the proton.

$$d^2\sigma^{CC}(e^-p)/dQ^2 \propto \int (u + c + (1-y)^2(\overline{d} + \overline{s}))dx$$

$$d^2\sigma^{CC}(e^+p)/dQ^2 \propto \int ((1-y)^2(d+s) + \overline{u} + \overline{c})dx$$

At low Q^2, the higher cross section for e^-p-scattering comes from the higher u-quark density compared to the d-quark density. The Q^2-dependence is given mainly by the kinematic factor $(1-y)^2$. Predictions of the Standard Model using the CTEQ4D [11] parametrization of the parton densities, as well as a ZEUS QCD fit, describe the cross section ratio well.

Extraction of the W mass : The charged current cross section depends on the mass of the W boson, M_W, and the Fermi coupling constant, G_F:

$$\frac{d\sigma^{CC}}{dQ^2} \propto \frac{G_F^2}{4\pi}\frac{M_W^4}{(M_W^2 + Q^2)^2}.$$

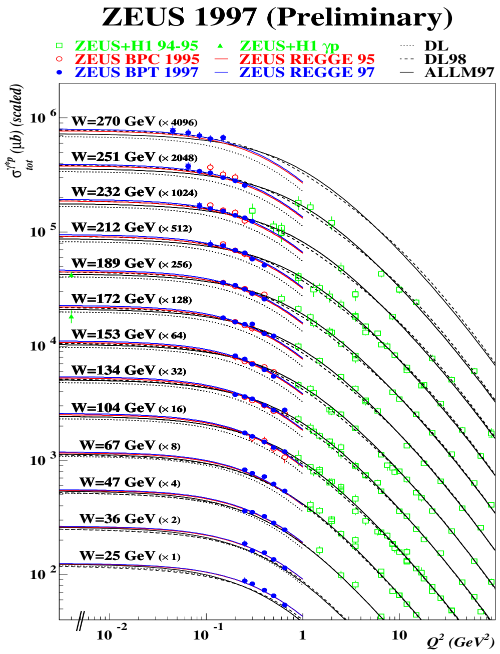

Figure 2. Total virtual photon-proton cross section extracted form the $F_2(x, Q^2)$ data at very low Q^2 shown together with ZEUS [5] and H1 [6] measurenments at higher Q^2 and directly measured photoproduction cross sections.

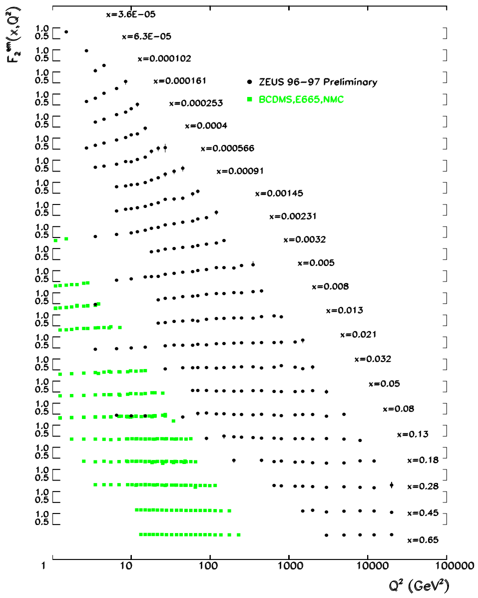

Figure 3. Preliminary $F_2(x, Q^2)$ values from the ZEUS 1997 data together with BCDMS [7], E665 [8], and NMC [9] data at lower Q^2 .

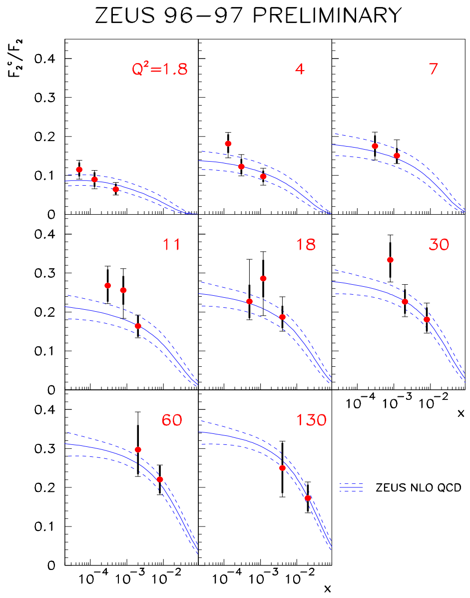

Figure 4. Contribution of charm to the total structure function $F_2(x, Q^2)$.

A fit of this function to the measured charged current cross section has been performed. The result is shown in Fig.6 in the $G_F - M_W$ plane, together with the 1 σ error contour of the fit. The resulting value for the W mass is :

$$M_W = 80.9 \ ^{+4.9}_{-4.6} \ (\mathrm{stat.}) \ ^{+5.0}_{-4.3} \ (\mathrm{syst.}) \ ^{+1.3}_{-1.2} \ (\mathrm{pdf}) \ \mathrm{GeV}.$$

The last error reflects the variation of the result due to different parton distribution functions used in the fit. In the Standard Model, the Fermi coupling constant is related to the W mass by :

$$G_F = \frac{\pi\alpha}{\sqrt{2}} \frac{M_Z^2}{M_W^2(M_Z^2 - M_W^2)} \frac{1}{1 - \Delta r(M_W)}.$$

This relation is shown in Fig.6 by the corresponding line. Assuming the validity of the Standard Model, using $G_F = 1.16639 \cdot 10^{-5}$ GeV^2 [12]

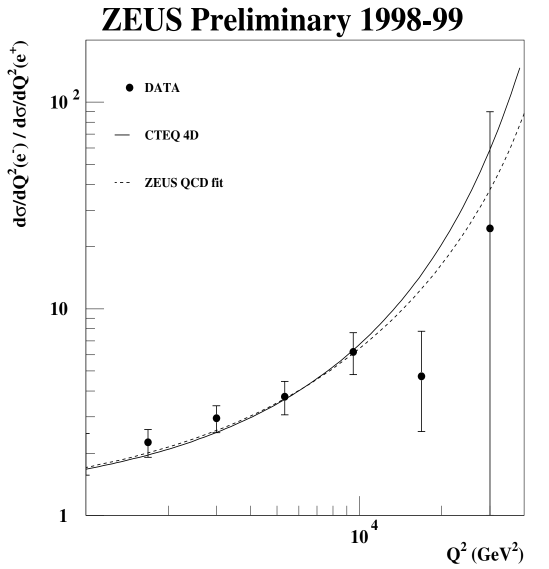

Figure 5. Ratio of charged current cross section for e^-p- to e^+p-scattering.

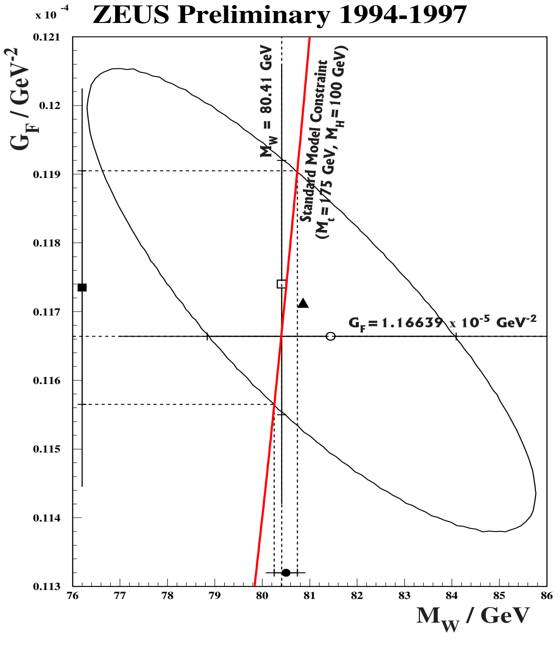

Figure 6. Result from the fit to the measured charged current cross section with G_F and M_W as parameters.

and for the radiative corrections, Δr, a Higgs mass of $M_H = 100$ GeV and a top mass of $M_T = 175$ GeV, the measured charged current cross section constrains the W mass to :

$$M_W = 80.50\ ^{+0.24}_{-0.25}\ (\text{stat.})^{+0.13}_{-0.15}\ (\text{syst.})\ ^{+0.30}_{-0.31}\ (\text{pdf})\ \text{GeV}.$$

This is a nice consistency check and demonstrates the sensitivity of the charged current cross section to the electroweak parameters of the Standard Model.

W production : The production of $W^\pm$ bosons has been studied in the process $e^+p \to e^+W^\pm X$ with subsequent leptonic decays: $W^\pm \to e^\pm\nu$ or $W^\pm \to \mu^\pm\nu$. Events from this reaction were identified by requiring a missing transverse momentum of more than 10 GeV and an isolated lepton in the final state. Three events were found, all consistent with the decay $W^+ \to e^+\nu$. The estimated background from other processes is one event. This results in a cross section for W production at HERA of :

$$\sigma(e^+p \to e^+W^\pm X) = 0.9\ ^{+1.0}_{-0.7}\ (\text{stat.})\ \pm 0.2\ (\text{syst.})\ \text{pb}.$$

Events with isolated leptons and high missing transverse momenta : The H1 collaboration has reported the observation of six events each containing an isolated lepton with high transverse momentum and a large missing transverse momentum in the final state [13]. The large rate of such events is not understood in the Standard Model. The ZEUS collaboration has also searched for such events. Three events were found, all with an isolated positron. From Monte Carlo studies of background processes one expects 3.4 ± 0.7 events with an $e^\pm$ and 1.9 ± 0.4 events with a $\mu^\pm$ final state. Hence, no evidence was found by ZEUS for an anomalous rate of events with an isolated lepton and high missing transverse momentum.

3. BEYOND THE STANDARD MODEL

Any kind of interaction with a energy scale much above the available center of mass energy would manifest itself as an effective contact interaction, like the four-fermion model in the case of the weak interaction at low energies. The most general Lagrangian for contact interactions contains scalar, vector, and tensor terms. Contributions from scalar and tensor terms are already constrained by previous experiments to be beyond the sensitivity at HERA. The effective Lagrangian for vector contact interactions has the following form :

$$L_{CI} = \sum_{\alpha,\beta=L,R} \eta^{eq}_{\alpha\beta} \cdot (\overline{e}_\alpha \gamma^\mu e_\alpha)(\overline{q}_\beta \gamma_\mu q_\beta),$$

with

$$\eta = \frac{\epsilon \cdot g^2_{CI}}{\Lambda^2} \text{ where } \epsilon = \pm 1.$$

Here g_{CI} is a coupling constant which by convention is taken as $g^2_{CI} = 4\pi$ and Λ is the typical scale of the interaction. The indices L,R denote the chirality of the fermions. Parity conservation and quark flavor symmetry lead to the following contraint :

$$\eta^{eq}_{LL} + \eta^{eq}_{LR} - \eta^{eq}_{RL} - \eta^{eq}_{RR} = 0.$$

The ZEUS collaboration has searched for contact interactions of the types shown in Fig.7. Fits of the Standard Model plus contact interaction terms have been performed on the complete dataset of 47.7pb^{-1} from e$^+$p interactions. The results of the fits are shown in Fig.8. For each investigated interaction combination the fitted $\frac{\epsilon}{\Lambda^2}$ values are shown. Given are also the 95% c.l. lower limits for the scale parameter Λ. The limits are in the range of several TeV.

Search for excited electrons : Contact interactions could be the manifestation of a substructure resulting from a new layer of fermions. If these fermions were composite objects then one could expect the existence of excited states, e.g excited positrons. They would be produced at HERA directly at the $e^+ - \gamma/Z$ vertex and would decay with a considerable branching fraction into $e^+ + \gamma$. A search for final states containing a high mass $e^+ + \gamma$ has been performed. For $e^+ + \gamma$ masses larger than 100 GeV, 7 events were found where 8.8 such events were expected from Standard Model background processes. This can be turned into limits of the coupling f/Λ as a function of an excited positron mass, where f is the

Model	η^{ed}_{LL}	η^{ed}_{LR}	η^{ed}_{RL}	η^{ed}_{RR}	η^{eu}_{LL}	η^{eu}_{LR}	η^{eu}_{RL}	η^{eu}_{RR}
VV	$+\eta$	$+\eta$	$+\eta$	$+\eta$	$+\eta$	$+\eta$	$+\eta$	$+\eta$
AA	$+\eta$	$-\eta$	$-\eta$	$+\eta$	$+\eta$	$-\eta$	$-\eta$	$+\eta$
VA	$+\eta$	$-\eta$	$+\eta$	$-\eta$	$+\eta$	$-\eta$	$+\eta$	$-\eta$
X1	$+\eta$	$-\eta$			$+\eta$	$-\eta$		
X2	$+\eta$		$+\eta$		$+\eta$		$+\eta$	
X3	$+\eta$			$+\eta$	$+\eta$			$+\eta$
X4		$+\eta$	$+\eta$			$+\eta$	$+\eta$	
X5		$+\eta$		$+\eta$		$+\eta$		$+\eta$
X6			$+\eta$	$-\eta$			$+\eta$	$-\eta$
U1					$+\eta$	$-\eta$		
U2					$+\eta$		$+\eta$	
U3					$+\eta$			$+\eta$
U4						$+\eta$	$+\eta$	
U5						$+\eta$		$+\eta$
U6							$+\eta$	$-\eta$

Figure 7. The terms of contact interactions which have been searched for by ZEUS.

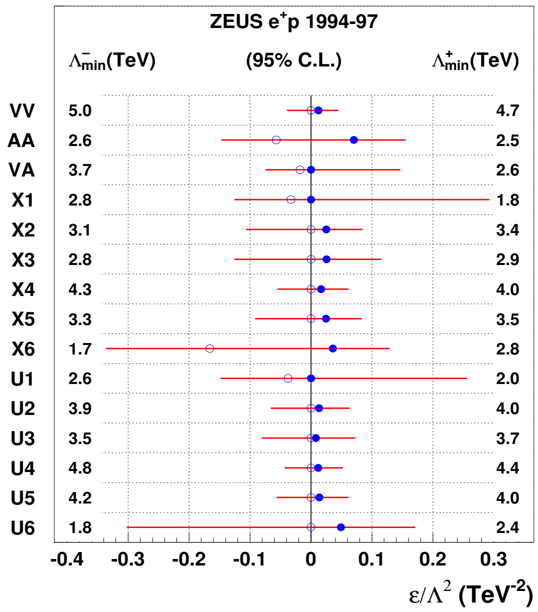

Figure 8. Results of the contact interaction search. The full circles and Λ^+_{min} correspond to $\epsilon = +1$, the open circles and Λ^-_{min} to $\epsilon = -1$. The labels to the left of the frame define the type of interaction as shown in Fig.7.

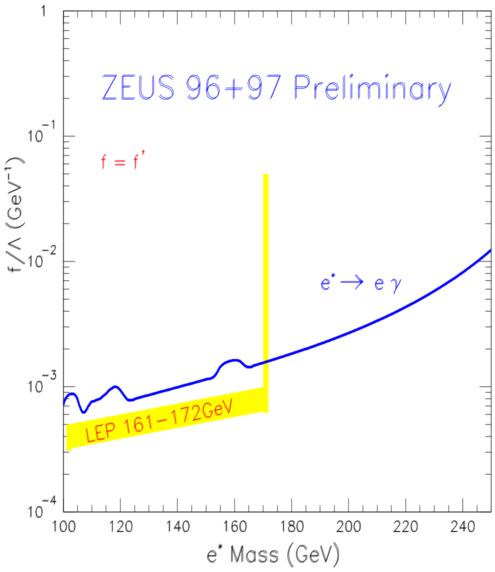

Figure 9. Limits on f/Λ of an excited positron versus the excited positron mass. Shown are also corresponding limits from LEP [14].

coupling strength and Λ is the mass scale. Figure 9 shows these limits and compares them to limits on excited electron production obtained at LEP [14]. Up to masses of the highest LEP energy, the ZEUS limits are slightly less restrictive than the LEP ones. The ZEUS limits extend, however, to higher values of the excited positron mass than can be reached by LEP.

Search for leptoquarks : HERA is an ideal collider to look for the production of leptoquarks because they can be formed directly in the s-channel : $e^+ + q \to LQ \to e^+ + jet$. Events were selected with positrons of more than 25 GeV and jets with transverse momenta of more than 10 GeV in the final state. For an effective mass of the positron-jet system, $M_{e-jet} > 200$ GeV, 68 events were found and 43^{+14}_{-12} were expected from Standard Model neutral current scattering. The angular distribution of the positron-jet system is close to the one expected from Standard Model neutral current events. It was concluded that no sign of leptoquark production was observed. This results in limits for the coupling strength of a possible leptoquark versus its mass for different types

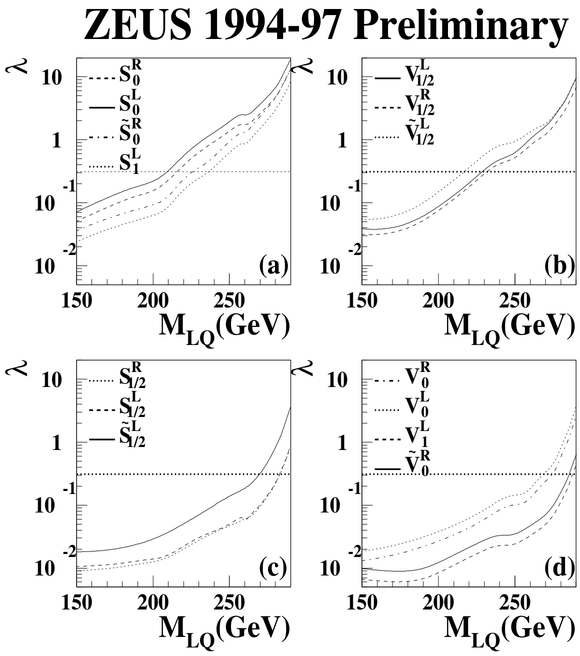

Figure 10. Limits on the couplings of leptoquarks versus the leptoquark mass mass for various types of scalar and vector leptoquarks.

of scalar and vector leptoquarks which are shown in Fig.10.

Search for R-parity violating SUSY : A particular kind of leptoquarks could arise in R-parity violating supersymmetry. If R-parity is not conserved supersymmetric leptosquarks can be formed at HERA. The ZEUS collaboration looked for their production with subsequent R-parity violating decays into eq and eqqq final states. The quarks would manifest themselves as jets. The search in the eq final state was done by requiring a positron with an energy of at least 15 GeV plus a jet with a transverse energy of at least 30 GeV. In the case of the eqqq final state, the required lepton energy was at least 15 GeV whereas the first two jets had to have transverse energies of at least 40 GeV and 20 GeV respectively. In the eq channel, 78 events were found and 88.6 events were expected from Standard Model background processes. In the eqqq channel, 33 events were found with 33.6 events expected. From these results, limits for the coupling , λ'_{ljk}, of an R-parity

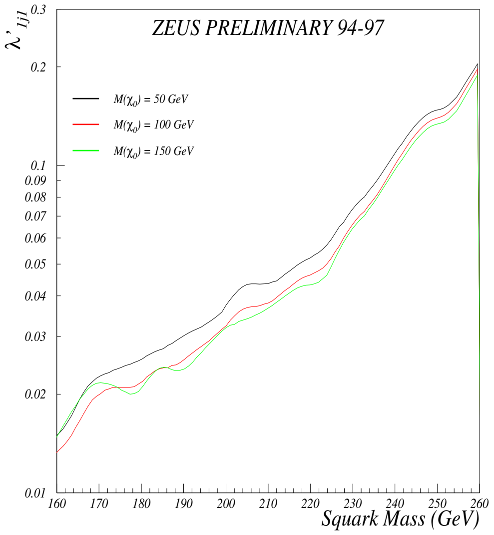

Figure 11. Limits for the coupling of an R-parity violating squark to positron and quark. The curves result from different assumptions on the mass of the lightest supersymmetric particle, χ_0.

violating squark to positron and quark were derived with several assumptions for the mass of the lightest supersymmetric particle, χ_0. These limits as a function of the squark mass are shown in Fig.11.

4. PROPERTIES OF FINAL STATES AND JETS

Fragmentation in DIS : The charged particle distribution in the current region of deep inelastic scattering events has been investigated in the Breit frame. For each charged particle in the current region, the momentum fraction $\mathrm{x_p} = 2\mathrm{p^{Breit}}/\mathrm{Q}$ was calculated, where $\mathrm{p^{Breit}}$ is the particle momentum in the Breit frame. Figure 12 shows the distribution of $1/\sigma_{\mathrm{tot}} \mathrm{d}\sigma/\mathrm{dln}(1/\mathrm{x_p})$ in various bins of Bjorken x and Q^2 . The curves are fits of distorted Gaussians of the form :

$$\frac{1}{\sigma_{\mathrm{tot}}}\frac{\mathrm{d}\sigma}{\mathrm{dln}(1/\mathrm{x_p})} \propto \exp\left(\frac{1}{8}\mathrm{k} - \frac{1}{2}\mathrm{s}\delta - \frac{1}{4}(2+\mathrm{k})\delta^2 + \frac{1}{6}\mathrm{s}\delta^3 + \frac{1}{24}\mathrm{k}\delta^4\right),$$

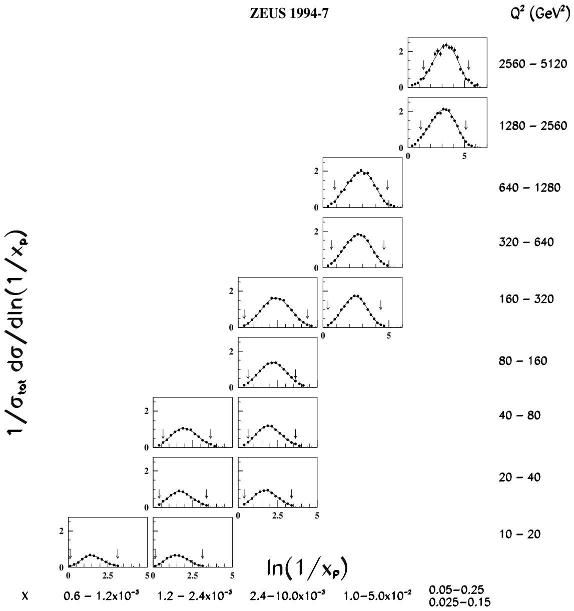

Figure 12. Charged particle distributions in the current region of the Breit frame. For the discription of the curves see text.

with $\delta = (\ln(1/\mathrm{x_p}) - 1)/\mathrm{w}$.

Here l=mean, w=width, s=skewness, and k=kurtosis are the moments of the distorted Gaussian. This form of the distribution is motivated by perturbative QCD calculations in the MLLA approximation. The arrows in Fig.12 indicate the fit regions. The moments of the fitted curves are presented in Fig.13 as functions of Q^2 for various x bins. Data from e^+e^- annihilation [17] are included for comparison. The measured moments are compared to calculations by Dokshitzer et al. [15] and by Fong and Webber [16]. The DIS and e^+e^- data show fair agreement. While the calculation of Dokshitzer et al. can describe the measured mean values, no model gives an acceptable description of the higher moments.

Determination of α_s : The presence of jets in the final state with hogh transverse momenta allows the use of perturbative QCD (pQCD) to calculate the rate and properties of such events. In particular, the rate of events with two jets

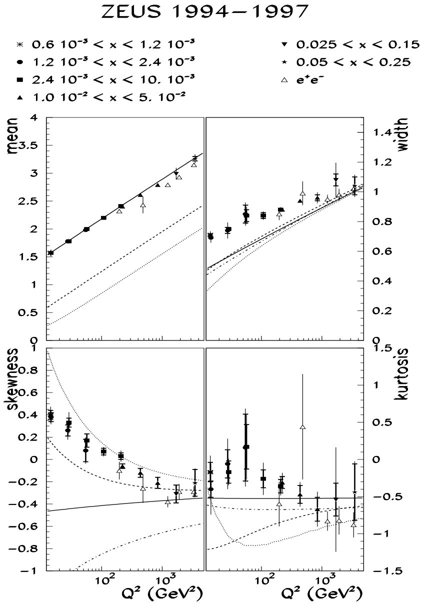

Figure 13. Moments of the charged particle distributions in the current region of the Breit frame.The curves are calculations of Dokshitzer et al. [15]: full line $Q_0 = \Lambda$, dashed line $Q_0 = 2\Lambda$, dotted line $Q_0 = 3\Lambda$, and of Fong and Webber [16] (dashed-dotted line).

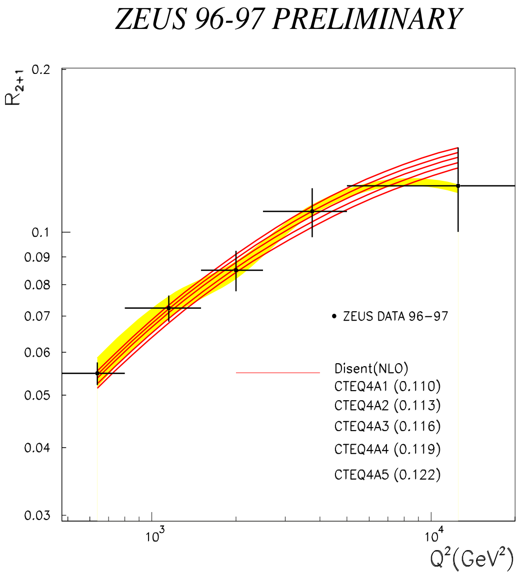

Figure 14. The fraction of two jet events in 5 different Q^2 bins. The curves are calculation with the DISENT program correseponding to different values of α_s.

plus the proton remnant can be expressed as an expansion in the strong coupling constant α_s : $\sigma_{2+1}(Q^2) = c_1 \cdot \alpha_s(Q^2) + c_2 \cdot \alpha_s^2(Q^2) + ...,$ where the coefficients c_i are calculable in pQCD. From a measurement of such dijet event rates one can hope to determine α_s. Events were selected in the kinematic region : $Q^2 > 470$ GeV^2 ; $-1 < \eta^{jet} < 2$; $E_T^{jet1}, E_2^{jet2} > 5$ GeV in the lab system and $E_T^{jet1} + E_T^{jet2} > 17$ GeV in the Breit frame. This is a region in which experimental and theoretical uncertainties, in particular the dependence on the renormalization scale, are small. In Fig.14 the measured ratios $R_{2+1}(Q^2) = \sigma_{2+1}(Q^2)/\sigma_{tot}(Q^2)$ are presented for 5 bins in Q^2 . Fitted to the data are curves which result from next to leading order QCD calculations with the program DISENT [18], using different values for α_s ranging from 0.110 to 0.122. This leads to α_s :

$$\alpha_s(M_Z) = 0.120 \pm 0.003 \text{ (stat.)} \\ {}^{+0.005}_{-0.006} \text{ (exp.) } {}^{+0.003}_{-0.002} \text{ (theory)}.$$

The virtual-photon structure : In addition to the normal "point-like" coupling directly to the quark charge, dominant at high Q^2 , the exchanged photon at low Q^2 can also fluctuate into partons, one of which then interacts with the proton. In the latter case, known as a "resolved-photon" interaction, not all of the photon's energy enters the hard scattering process. Experimentally, the fraction of the photon's energy in the hard scattering is given by :

$$x_\gamma^{obs} = \frac{\sum_{jets} E_T e^{-\eta}}{2yE_e} \cong \frac{(E - p_z)_{jets}}{(E - p_z)_{total}}.$$

For direct photon interactions, x_γ^{obs} should be close to 1. Experimentally, a direct-enriched event sample is defined by $x_\gamma^{obs} > 0.75$ and a resolved-enriched sample by $x_\gamma^{obs} < 0.75$. It is expected that the resolved contribution decreases and eventually vanishes with increasing Q^2 . Figure 15 shows the experimentally determined ratio $\sigma(x_\gamma^{obs} < 0.75)/\sigma(x_\gamma^{obs} > 0.75)$. The resolved contribution decreases with Q^2 , as expected, but at

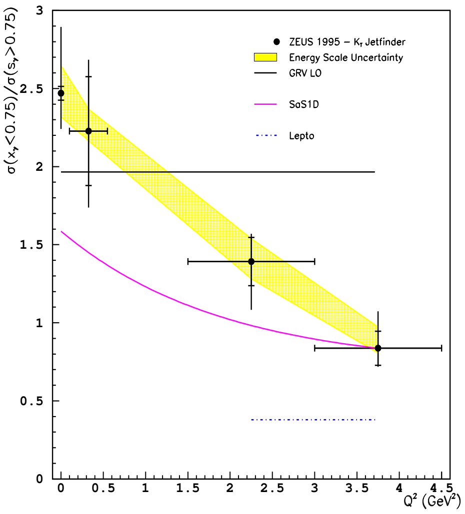

Figure 15. The fraction of resolved to direct photon interactions as a function of Q^2 .The solid horizontal line is a predictionts from a HERWIG MC simulation using the GRV LO parametrization of the photon, the dashed-dotted horizontal line is a LEPTO MC prediction, and the solid curve is from a HERWIG MC simulation with the SaS1D [19] parametrization of the photon.

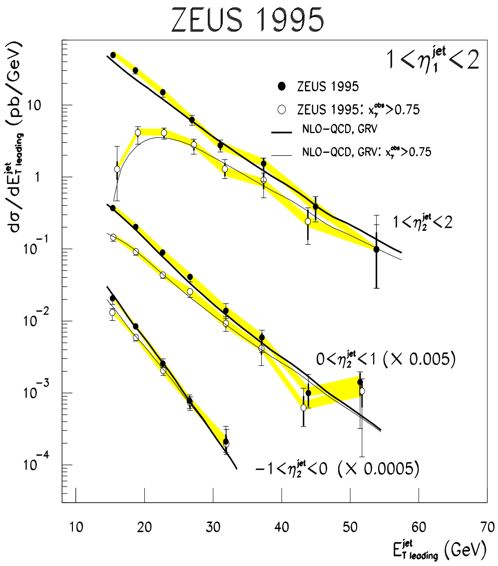

Figure 16. Phoroproduction of dijet events as a function of the transverse energy of the leading jet for different pseudorapidity intervals of the jets.

Q^2 =4 GeV^2 its contribution is still as big as the direct one. This behavior cannot be explained by any of the models shown in Fig.15.

Photoproduction of jets : The photoproduction of dijet events has been studied for jet transverse energies of $E_T^{jet1} > 14$ GeV and $E_T^{jet2} > 11$ GeV in the range $x \approx 10^{-2} - 10^{-1}$. Results are shown in Fig.17 for different pseudorapidity intervals of the jets. A comparison with NLO QCD calculations shows in general good agreement. However, when both jets go forward, $1 < \eta^{jet1,2} < 2$, and the transverse energy of the leading jet is below 25 GeV the data are above the NLO calculations. Photoproduction events with jets of transverse energies $E^{jet} > 15$ GeV have been used to study the substructure of jets. For a given jet, a k_T-cluster algorithm has been used to find subjets. The clustering was stopped when the variable $d_{ij} = \min(E_T^i, E_T^j)^2 \cdot (\Delta\eta_{ij}^2 + \Delta\phi_{ij}^2)$ reached a value $d_{cut} = y_{cut} \cdot (E_T^{jet})^2$. The remaining clusters were called subjets. Their number depends on the value of d_{cut}. The average number of subjets, $< n_{subjet} >$, is plotted in Fig.16 against η^{jet} for $y_{cut} = 0.01$. The average number of subjets can be described by both the PYTHIA and HERWIG Monte Carlo calculations. Monte Carlo calculations with only quark jets and with only gluon jets in the final state are also shown. When the jet goes backwards (negative η), it is close to the expectations from quark jets only. When the jet goes forwards (positive η), the average number of subjets approaches the predictions for gluon jets only. The observed behavior can be qualitatively explained by the fact that the direct boson-gluon-fusion process produces two quark jets and dominates in the backward direction, whereas contributions from resolved processes dominate in the forward direction. They produce gluon jets as well as quark jets and the gluon jets tend to go forward.

Photoproduction of charm and beauty : Processes in which heavy quarks are produced in the final state are generally considered to be calculable in pQCD because the quark mass provides a hard scale. The ZEUS collaboration analyzed new data on photoproduction of inclusive

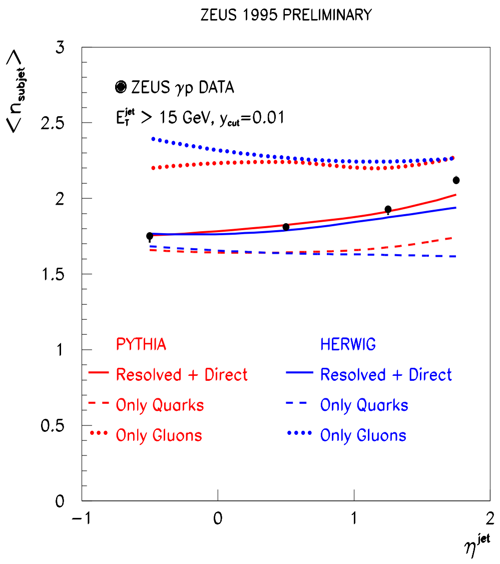

Figure 17. Average number of subjets in jets with $E_T^{\rm jet} > 15$ GeV. The curves correspond to MC calculation with HERWIG and PYTHIA : solid line - resolved+direct contributions ; dashed line - only quarks in the final state ; dotted line - only gluons in the final state.

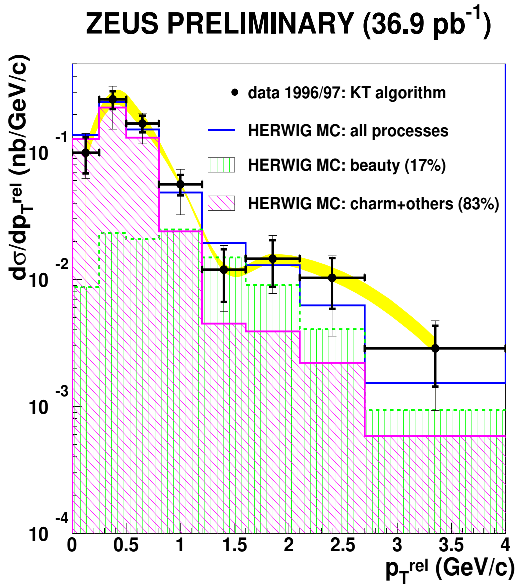

Figure 18. Distribution of the relative transverse momentum, $p_T^{\rm rel}$ of electrons w.r.t. the nearest jet axis.

D* mesons at low photon-proton center-of-mass energies. The differential cross section as functions of $p_T^{D^*}$ and η^{D^*} do not agree well with NLO calculations by Frixione et al. [20].
The photoproduction of heavy quarks is expected to be dominated by photon-gluon-fusion processes. The production of b-quarks has been studied in two-jet events plus an electron, hypothesized to originate from the semileptonic decay of one of the b-quarks. Each jet was required to have transverse energy of more than 7.5 GeV and the decay electron candidate must have a transverse momentum of more than 1.6 GeV. In such events, the electron is very close to or inside one of the jets. To identify such electrons the dE/dx information from the central tracking detector of ZEUS has been used. Figure 18 shows the measured distribution of $p_T^{\rm rel}$, the relative transverse momentum of the electron to the nearest jet axis. The measurement is compared to results from three HERWIG Monte Carlo simulations: all process simulated; all processes simulated except b-quark production; and simulation of b-quark production alone. The simulation including all processes gives a good description of the data. At higher $p_T^{\rm rel}$, the contribution from b-quark production is needed to describe the spectrum; the fraction of b-quark production is determined to be $(20 \pm 6 \ ^{+12}_{-7})$ %. The preliminary visible cross section for the production of two jets and one electron from a b-quark decay is $\sigma_{e^+p\to e^- +2jets+X} = 39 \pm 11 \ ^{+23}_{-15}$ pb. Although HERWIG describes the shape of the data the measured visible cross section is about a factor of two higher than predicted by HERWIG.

5. DIFFRACTION

Spin density matrix for exclusive ρ^0 production : The exclusive production of ρ^0 mesons, $e^+p \to \rho^0 p$, has been studied for $3 < Q^2 < 30$ GeV^2 and $40 < W < 120$ GeV. The ρ^0 mesons were detected by their decay into two charged pions. The ρ^0 production and decay process is described by three angles : the angle Φ_h between the scattering plane and the ρ^0 produc-

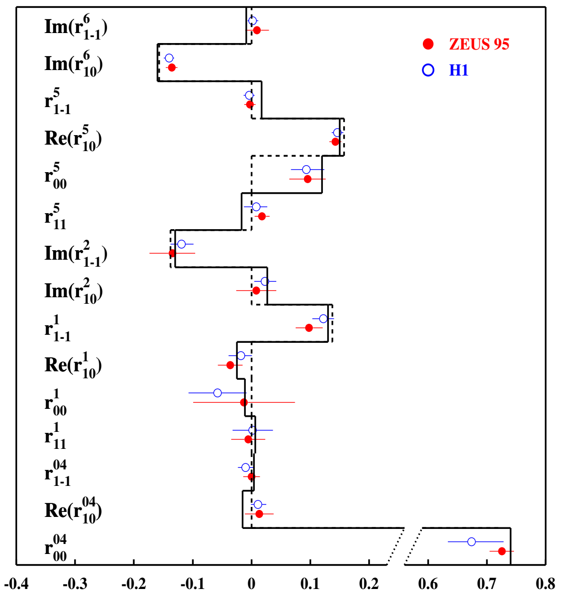

Figure 19. Fitted density matrix elements for the production and decay angular distributions of exclusive ρ^0 production. The dashed line is the SCHC prediction. The solid line is a pQCD calculation [22].

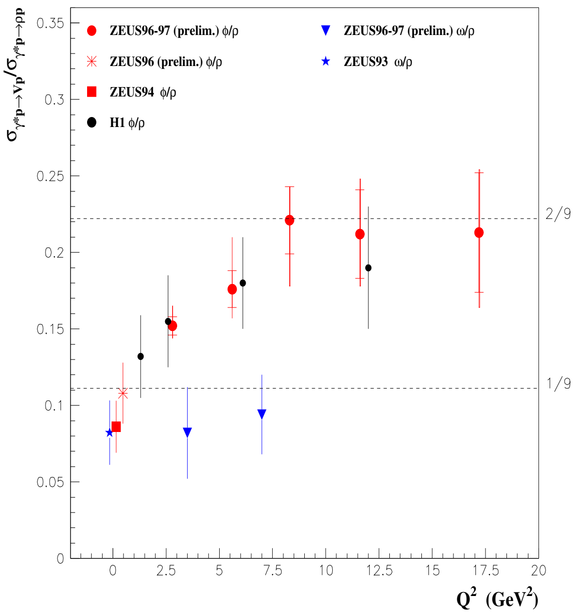

Figure 20. Ratios of exclusive ϕ and ω production to ρ^0 production in diffractive DIS events. The U(4) prediction of 2/9 and 1/9 respectively are also shown.

tion plane, the angle ϕ_h between the production plane and the ρ^0 decay plane, and the angle Θ_h between the positive pion in the ρ^0 rest system and the direction of flight of the ρ^0. Under the assumption of parity conservation and a hermitian spin density matrix, the distribution of these three angles, $W(\Phi_h, \phi_h, \Theta_h)$, depends on 15 spin density matrix elements. The distributions of the three angles have been measured and a simultaneous fit of the 15 density matrix elements to the data has been performed. The result is shown in Fig.19 together with results from the H1 collaboration [21]. The data are compared to the prediction of s-channel helicity conservation (SCHC) and to a prediction from a pQCD calculation [22]. SCHC predicts the dotted line in the figure and predicts that five density matrix elements can be different from zero. There is a clear discrepancy between the SCHC prediction and the data for r^5_{00}. This density matrix element depends on the helicity flip amplitude from a transverse (helicity=1) photon to a ρ^0 with helicity zero. The pQCD prediction is in agreement with the measurement of r^5_{00}. The size of the helicity flip amplitude needed to explain the data is only a few percent of the total SCHC amplitude.

Ratios of exclusive vector meson production : Assuming U(4)-symmetry, i.e. neglecting differences in the masses of the quarks, the ratios of the exclusive production cross section for different vector mesons should be determined only by the coupling of the photon to the charges of the quarks, in particular the production of light vector mesons should be in the ratio $\rho : \omega : \phi = 9 : 1 : 2$. In photoproduction processes, this relation does not hold. The ZEUS collaboration has measured the total cross section for exclusive ω production in DIS. Data on exclusive ρ^0 and ϕ production are available from previous measurements of ZEUS [23] and H1 [24]. Ratios of exclusive vector meson production as a function of Q^2 are shown in Fig.20. The ratio of $\sigma_{\gamma^* p \to \phi p}/\sigma_{\gamma^* p \to \rho^0 p}$ approaches the U(4) prediction of 2/9 for Q^2 values greater than about 7 GeV^2. For $\sigma_{\gamma^* p \to \omega p}/\sigma_{\gamma^* p \to \rho^0 p}$, the values at low Q^2 are already close to the U(4) prediction of

1/9.

Charm cross section for diffractive events : ZEUS has previously reported a measurement of the cross section for the process $\sigma(e^+p \to e^+pD^*X)$ with subsequent decays of $D^* \to \pi D^0$; $D^0 \to K\pi$ in diffractive reactions. The inclusive D^* production cross section for diffractive events has also been determined from the $D^* \to \pi D^0$; $D^0 \to K3\pi$ decay channel. The kinematic region of this measurement is :

$1 < Q^2 < 600\ \mathrm{GeV}^2,\ 0.04 < y < 0.7,,$
$2 < p_T(D^*) < 9\ \mathrm{GeV}^2,\ |\eta(D^*)| < 1.5,$
$x_{\mathbb{P}} < 0.015,$ and $\beta < 0.8.$

The cross section for this kinematic region is :

$$\sigma(e^+p \to e^+pD^*X) = 526 \pm 109\ (\mathrm{stat.})\ {}^{+203}_{239}\ (\mathrm{syst.})\ \mathrm{pb}.$$

The two measurements can be compared by extrapolation to the kinematical region of the previous mesurement from the $D^0 \to K\pi$ decay channel:

$$\sigma(e^+p \to e^+pD^*X) = 398 \pm 83\ (\mathrm{stat.})\ {}^{+154}_{-180}\ (\mathrm{syst.})\ \mathrm{pb}$$

from $D^0 \to K3\pi$ decay mode,

$$\sigma(e^+p \to e^+pD^*X) = 379 \pm 66\ (\mathrm{stat.})\ {}^{+99}_{-140}\ (\mathrm{syst.})\ \mathrm{pb}$$

from $D^0 \to K\pi$ decay mode.

The two measurements are in good agreement. The ratio of diffractive to total D^* production is $(8.9 \pm 2.4\ {}^{+1.7}_{-1.6})\%$ as determined from the $D^0 \to K3\pi$ decay mode.

Diffractive cross section at low Q^2 : The diffractive cross section has been determined from events for which the scattered positron was measured in the beam pipe calorimeter and in the beam pipe tracker. The selection of the diffractive events was performed with the $\ln M_x^2$ method [25]. The diffractive cross sections as a function of W for different Q^2 and M_x intervals are presented in Fig.21. The value of $\alpha_{\mathbb{P}}$ has been extracted from the W-dependence of the diffractive cross-section and extrapolated to t=0 using a slope of

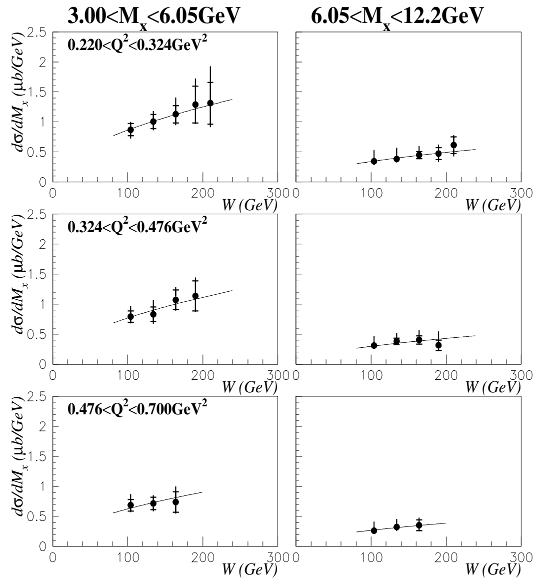

Figure 21. Diffractive cross sections $d\sigma/dM_x$ from the ZEUS BPC data.

the Pomeron trajectory of $0.25\ \mathrm{GeV}^{-2}$. The resulting $\alpha_{\mathbb{P}}(0)$ is plotted in Fig.22 together with other measurements of ZEUS [26] and H1 [27] at different Q^2 and together with a prediction of the ALLM parametrization [3]. There is fair agreement between the measurements. The ALLM parametrization describes qualitatively the trend of the data.

Events with leading baryons : The ZEUS leading proton spectrometer (LPS) tags events in which the final state contains a proton which is scattered at a very small angle and carries a sizeable fraction ,x_L, of the incoming proton's energy. The accepted kinematic region for such leading protons is given by $x_L \geq 0.4$ and transverse momenta $p_t \leq 1$ GeV. Diffractive events are concentrated mainly at $x_L > 0.97$. For $x_L < 0.97$, Reggeon exchange, mostly π^0 and f^0, dominates. From the LPS tagged events with $x_L < 0.97$, the ratio of the leading proton structure function, $F_2^{LP(4)}(x, Q^2, x_L, p_t^2)$, to the total structure function $F_2(x, Q^2)$ has been determined. Figure 23 shows this ratio for $0.61 < x_L < 0.73$ and various x and Q^2 bins. The measured ratios are flat

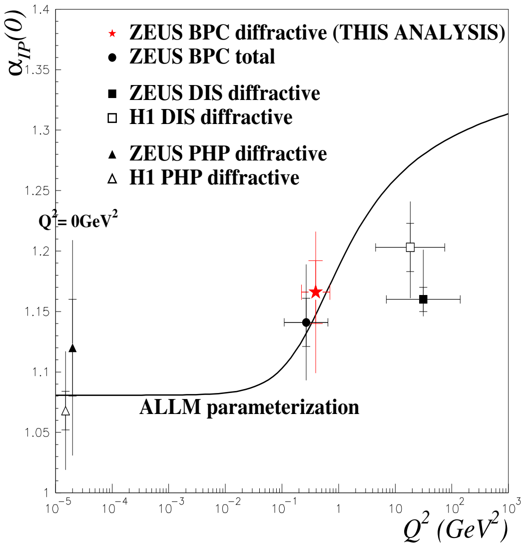

Figure 22. The intercept of the Pomeron trajectory as a function of Q^2 . The result of the ZEUS BPC data analysis is shown together with other ZEUS [26] and H1 [27] results. The measurements are compared to a prediction from the ALLM parametrization [3].

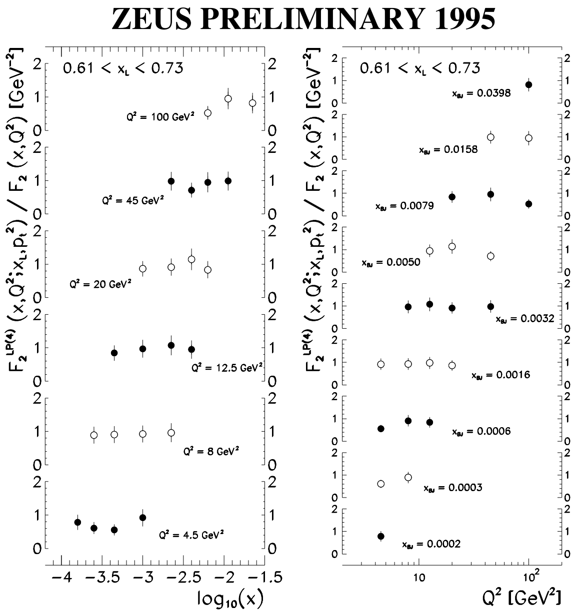

Figure 23. Ratio of the leading proton structure function $F_2^{LP(4)}$ to $F_2(x,Q^2)$ as functions of x and Q^2 for $x_L < 0.97$.

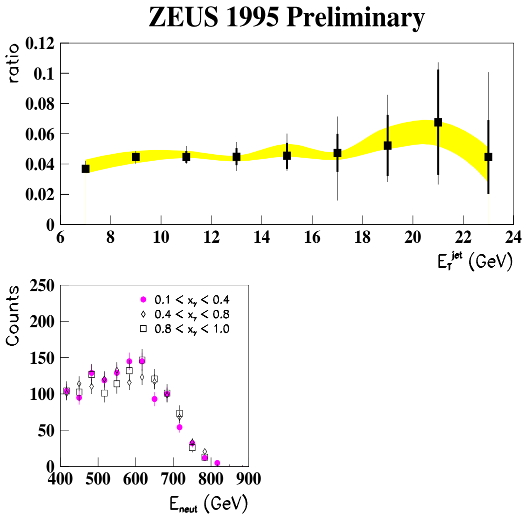

Figure 24. Ratio of dijet+leading-neutron events to all dijet photoproduction events and neutron energy spectra for resolved photoproduction events.

fuctions of x and Q^2 . This indicates that the interaction at the proton vertex seems to be independent of the variables (x,Q^2) at the positron vertex. This is a confirmation of the factorization hypothesis for diffractive and leading proton events. Very similar results have been obtained for events with leading neutrons. Leading neutrons have been detected by the ZEUS forward neutron calorimeter (FNC). It accepts neutrons which are produced at angles very close to zero. The ratio of dijets+leading-neutron events to all dijet events has been determined for FNC-tagged photoproduction. This ratio is shown in Fig.24 as a function of the transverse jet energy. It is essentially flat. Also shown in Fig.24 are neutron energy spectra for resolved photoproduction events for three ranges of x_γ. The spectra are identical within errors. These results also confirm the factorization hypothesis.

Event shapes of diffractive events : Diffractive events have been identified by detecting the scattered proton in the ZEUS leading proton spectrometer (LPS). The events were selected in the

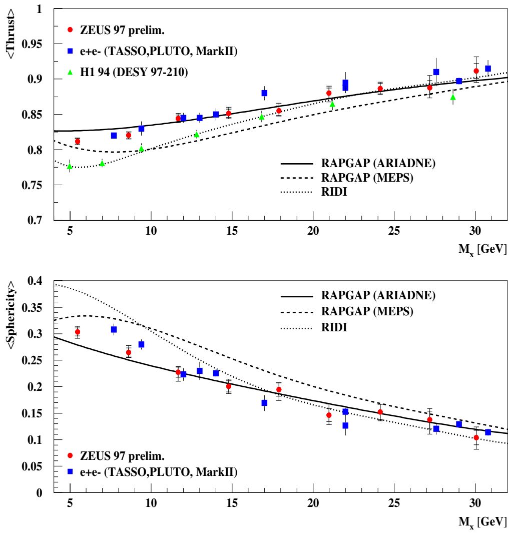

Figure 25. Average thrust and average sphericity in the photon-Pomeron rest frame for ZEUS LPS tagged events.Shown are also data from H1 [28], from e^+e^- scattering [29][30][31], and comparisons with Monte Carlo simulations.

region :

$4\ \mathrm{GeV}^2 < Q^2 < 90\ \mathrm{GeV}^2$ and
$4\ \mathrm{GeV} < M_x < 35\ \mathrm{GeV}$.

The final state was transformed into the photon-Pomeron center-of-mass system. In this system, the thrust and the sphericity were calculated for each event. The average thrust and the average sphericity of the diffractive events are shown in Fig.25 as functions of the invariant mass, M_x, of the dissociated photon. The increase of the average thrust and the decrease of the average sphericity with M_x indicate the development of a back-to-back two jet system in the photon-Pomeron rest frame. The ZEUS data are compared to H1 measurements [28] and to results from e^+e^- scattering data [29][30][31]. There is good agreement between the ZEUS and the e^+e^- scattering data for the average thrust and fair agreement for the average sphericity. The H1 data for the average thrust differ from the ZEUS data at lower M_x values. The data are also compared to Monte Carlo simulations. The RAPGAP program in combination with ARIADNE reproduces the ZEUS measurements well. RAPGAP with MEPS as well as RIDI, a two gluon exchange model, fail at lower M_x values for the ZEUS data. RIDI is able to describe the H1 data for the average thrust.

6. SUMMARY

The increased amount of data from the 1996-1997 running period and detector improvements have allowed an increase in the kinematic region accessible to measurements.
In the very low Q^2 region, the data approach smoothly the real photoproduction measurements.
The increased amount of data enables the study of jets in kinematic regions where experimental uncertainties become smaller and where the predictions of perturbative QCD calculations are supposed to be more reliable.
Comparisons between e^+p and e^-p scattering cross sections at high Q^2 were presented with substantial statistics. Many more data and results can be expected by the end of the 1999 data taking period.
Diffractive physics is a very lively area. The increased amount of data with LPS tagged events begins to allow a detailed analysis of final states from photon dissociation at higher invariant masses.

REFERENCES

1 A. Donnachie and P. Landshoff, Z. Phys. **C61** (1994) 139.
2 A. Donnachie and P. Landshoff, Phys. Lett. **B437** (1998) 408.
3 H.A. Abramovicz and A. Levy, DESY 97-251.
4 ZEUS Collab, J. Breitweg et al., E. Phys. J. **C7** (1999) 609.
5 ZEUS Collaboration, M. Derrick et al., Phys. Lett. **B293** (1992) 465.
6 H1 Collaboration, T. Ahmed et al., Phys. Lett. **B299** (1993) 374.
7 BCDMS Collaboration, A.C. Benvenuti et

al., Phys. Lett. **B223** (1989) 485; Phys.Lett. B237 (1990) 592.
8 E665 Collaboration, M.R. Adams et al., Phys. Rev. Lett. **D54** (1996) 3006.
9 NMC, M. Arneodo et al., Nucl. Phys. **B437** (1997) 3.
10 B.W. Harris and J. Smith, Phys. Rev. **D57** (1998) 2806.
11 CTEQ Collaboration, H.L. Lai et al., Phys. Rev. **D55** (1997) 1280.
12 Particle Data Group, C. Caso et al., E. Phys.J. **C3** (1998) 1.
13 H1 Collaboration, C. Adloff et al., E. Phys. J. **C5** (1998) 575.
14 L3 Collaboration, M. Acciari et al., Phys. Lett. **B401** (1997) 139; ALEPH Collaboration, contributed paper 615 to EPS HEP Conference, Jerusalem, 19-26 August 1997; DELPHI Collaboration, F.Barão et al., contributed paper 351 to EPS HEP Conference, Jerusalem 19-26 August 1997; OPAL Collaboration, K. Ackerstaff et al., E. Phys. J. **C1** (1998) 45.
15 Yu. Dokshitzer, V. Khoze and S. Troyan, Int. J. Mod. Phys **A7** (1992) 1875.
16 C.P. Fong and B.R. Webber, Phys. Lett. **B229** (1989) 289; Nucl. Phys. **B355** (1991) 54.
17 OPAL Collaboration, M. Akrway et al., Phys. Lett. **B247** (1990) 617; TASSO Collaboration, W. Braunschweig et al., Z. Phys. **C22** (1984) 307; Z. Phys. **C47** (1990) 187; TOPAZ Collaboration, R. Itoh et al., Phys.Lett. **B345** (1995) 335.
18 S. Catani and M.H. Seymour, Nucl. Phys. **B485** (1997) 291.
19 G.A. Schuler and T.Sjöstrand, Phys. Lett. **B376** (1996) 193.
20 S. Frixione et al., Phys. Lett. **B348** (1995) 633; Nucl. Phys. **B454** (1995) 3.
21 H1 Collaboration, C.Adloff et al., DESY 99-010, hep-ex/9902019, submitted to E. Phys. J. **C**.
22 D.Yu. Ivanov and R. Kirschner, Phys. Rev. **D58** (1998) 114.
23 ZEUS Collaboration, M. Derrick et al., Phys. Lett. **B356** (1995) 601; Phys. Lett. **B377** (1996) 259; Z. Phys **C73** (1996) 73; ZEUS Collaboration, J. Breitweg et al., E. Phys. J. **C6** (1999) 603.
24 H1 Collaboration, S. Aid et al., Nucl. Phys. **B463** (1996) 3; Nucl. Phys. **B468** (1996) 3; H1 Collaboration, C. Adloff et al., Z. Phys. **C75** (1997) 607; DESY 99-010, hep-ex/9902019, submitted to E. Phys. J.
25 ZEUS Collaboration, J. Breitweg et al., E. Phys. J. **C6** (1999) 43.
26 ZEUS Collaboration, M. Derrick et al., Z. Phys. **C69** (1996) 607; ZEUS Collaboration, J.Breitweg et al., Z. Phys. **C75** (1997) 421.
27 H1 Collaboration, C. Adloff et al., Z. Phys. **C74** (1997) 221; Z. Phys. **C76** (1997) 613.
28 H1 Collaboration, C. Adloff et al., E. Phys. J. **C1** (1998) 495.
29 TASSO Collaboration, W. Braunschweig et al., Z. Phys. **C47** (1990) 187.
30 PLUTO Collaboration, C. Berger et al., Z. Phys. **C12** (1982) 297.
31 MarkII Collaboration, A. Peterson et al., Phys. Rev. **D37** (1988) 1.